PLOS ONE

RESEARCH ARTICLE

Application of Electron Paramagnetic Resonance (EPR) Oximetry to Monitor Oxygen in Wounds in Diabetic Models

Céline M. Desmet[1], Aurore Lafosse[2,3], Sophie Vériter[2], Paolo E. Porporato[4], Pierre Sonveaux[4], Denis Dufrane[2], Philippe Levêque[1], Bernard Gallez[1]*

1 Biomedical Magnetic Resonance Research Group, Louvain Drug Research Institute, Université catholique de Louvain, Brussels, Belgium, **2** Endocrine Cell Therapy Unit, Center of Tissue/Cell Therapy, Institut de Recherche Expérimentale et Clinique, Cliniques Universitaires Saint-Luc, Université catholique de Louvain, Brussels, Belgium, **3** Plastic and Reconstructive Surgery Unit, Cliniques Universitaires Saint-Luc, Université catholique de Louvain, Brussels, Belgium, **4** Pole of Pharmacology, Institut de Recherche Expérimentale et Clinique, Université catholique de Louvain, Brussels, Belgium

* bernard.gallez@uclouvain.be

Citation: Desmet CM, Lafosse A, Vériter S, Porporato PE, Sonveaux P, Dufrane D, et al. (2015) Application of Electron Paramagnetic Resonance (EPR) Oximetry to Monitor Oxygen in Wounds in Diabetic Models. PLoS ONE 10(12): e0144914. doi:10.1371/journal.pone.0144914

Editor: Dariush Hinderberger, Martin-Luther-Universität Halle-Wittenberg, GERMANY

Received: August 25, 2015

Accepted: November 26, 2015

Published: December 14, 2015

Data Availability Statement: All relevant data are within the paper and its Supporting Information files.

Funding: This work was supported by a Starting Grant from the European Research Council (ERC No. 243188 TUMETABO to Pierre Sonveaux) and an Action de Recherche Concertée from the Communauté Française de Belgique (ARC 14/19-058). P.S. is a Research Associate and P.E.P. a Postdoctoral Fellow of the Fonds National de la Recherche Scientifique (F.R.S.-FNRS). The funders had no role in study design, data collection and

Abstract

A lack of oxygen is classically described as a major cause of impaired wound healing in diabetic patients. Even if the role of oxygen in the wound healing process is well recognized, measurement of oxygen levels in a wound remains challenging. The purpose of the present study was to assess the value of electron paramagnetic resonance (EPR) oximetry to monitor pO_2 in wounds during the healing process in diabetic mouse models. Kinetics of wound closure were carried out in streptozotocin (STZ)-treated and db/db mice. The pO_2 was followed repeatedly during the healing process by 1 GHz EPR spectroscopy with lithium phthalocyanine (LiPc) crystals used as oxygen sensor in two different wound models: a full-thickness excisional skin wound and a pedicled skin flap. Wound closure kinetics were dramatically slower in 12-week-old db/db compared to control (db/+) mice, whereas kinetics were not statistically different in STZ-treated compared to control mice. At the center of excisional wounds, measurements were highly influenced by atmospheric oxygen early in the healing process. In pedicled flaps, hypoxia was observed early after wounding. While reoxygenation occurred over time in db/+ mice, hypoxia was prolonged in the diabetic db/db model. This observation was consistent with impaired healing and microangiopathies observed using intravital microscopy. In conclusion, EPR oximetry using LiPc crystals as the oxygen sensor is an appropriate technique to follow wound oxygenation in acute and chronic wounds, in normal and diabetic animals. Nevertheless, the technique is limited for measurements in pedicled skin flaps and cannot be applied to excisional wounds in which diffusion of atmospheric oxygen significantly affects the measurements.

analysis, decision to publish, or preparation of the manuscript.

Competing Interests: The authors have declared that no competing interests exist.

Introduction

Wound healing is a complex phenomenon that is described schematically by 3 overlapping phases: inflammatory, proliferative and remodeling. During the first phase, inflammatory cells like neutrophils and monocytes are recruited into the wound to prevent infections and to clean the wound from dead tissue and other foreign bodies. The next step is characterized by the proliferation of cells to form new tissue: fibroblasts and endothelial cells (neovascularization) that form granulation tissue; and keratinocytes that proliferate and migrate to restore the epithelium (reepithelialization). The last step is the remodeling of the extracellular matrix that increases the wound tensile strength [1, 2]. In an acute wound, the sequence of these events is well represented and results in the restoration of anatomic and functional integrity of the tissue [3]. But, on the contrary, chronic wounds like diabetic ulcers, venous ulcers and other pressure sores [4] fail to restore the integrity of the tissue due to a dysregulation of this well-orchestrated process [3]. Etiologies of chronic wounds are multifactorial but one common factor observed in impaired wound healing is tissue hypoxia [4, 5].

Oxygen plays an important role at the several levels of the wound healing process [5–7]. First, during the inflammatory phase, oxygen is used by NADPH oxidases to produce reactive oxygen species (ROS) for oxidative burst [8]. During the proliferative phase, oxygen is used for oxidative phosphorylation in order to produce sufficient energy for proliferating cells with high metabolic need. Finally, oxygen is necessary for mature collagen production and deposition by fibroblasts during proliferative and remodeling phases. Indeed, hydroxylation of proline and lysine residues of procollagen chains is necessary to stabilize the triple helix of collagen. This reaction is catalyzed by hydroxylases and requires oxygen, iron, ascorbic acid and α-ketoglutarate as cofactors [9]. Consequently, prolonged hypoxia can be deleterious at each phase of the wound healing process: wounds suffering from poor oxygenation typically present a sustained inflammatory phase, a prolonged proliferative phase and/or a poor wound tensile strength [6].

While oxygen is known to play a key role in wound healing, there are only few experimental studies aimed at measuring oxygen in acute wounds and none in chronic wounds. The reason is that, to date, no method has been validated to measure pO_2 non-invasively, reliably and repeatedly in a wounded tissue. The use of polarographic Clark electrodes is the gold standard method to measure tissue oxygenation [6] but has several drawbacks. This method is invasive and the introduction of electrodes by itself modifies tissue environment by inducing injuries. Also, these electrodes consume oxygen during the measurements. Furthermore, reliable longitudinal studies of oxygenation are impossible because electrodes cannot be placed exactly at the same location on consecutive days. Hunt and his group, who were the first to study oxygenation in wound healing, developed subcutaneously implanted wire mesh cylinders and adapted subcutaneous tonometers for oxygen tension measurements in wounds [10]. The first technique is based on measurement of oxygen tension in the wound fluid aspirated from the dead wound space created by implantation of cylinders in the dorsal skin of animals [11, 12]; the second consists in the measurement of oxygen in the effluent of deoxygenated Ringer's lactate or saline perfused within the subcutaneously implanted tonometer. However, these techniques also suffer from some disadvantages. Implantation of cylinders or tonometers is complex and invasive and measurements in the aspirated wound fluid can easily be influenced by air bubbles contamination. More recently, the luminescence technique was used to image wound pO_2. Using films containing luminescent optical oxygen sensor, maps of surface wound pO_2 were obtained by Schreml and his group in human wounds [13, 14] whereas Li *et al.* measured transdermal pO_2 in burn wounds and skin grafts in pigs with oxygen-sensing paint-on bandages [15].

EPR oximetry could be a promising technique to measure wound pO_2 as it overcomes principal disadvantages of the methods previously cited. EPR oximetry is a technique based on the paramagnetic properties of oxygen. The interaction between unpaired electrons of oxygen and some paramagnetic probes, such as lithium phthalocyanine (LiPc), shortens the T_2 relaxation time which is related to a broadening of the EPR spectrum recorded from the probe. Line width broadening is directly proportional to the surrounding oxygen concentration, so that with appropriate calibration tissue pO_2 can be determined from the line width of the spectrum recorded from the paramagnetic oxygen sensor previously implanted in the tissue [16–19]. This technique presents the advantage to be minimally invasive: once the oxygen sensor is implanted in the tissue, EPR spectra can be recorded non-invasively *in vivo* using a low frequency (L-band) EPR spectrometer [17, 18]. Measurements can be recorded at the same location repeatedly during a long period of time [18] up to at least 5 years [20], allowing longitudinal studies. Moreover, the technique does not consume oxygen contrarily to microelectrodes and, consequently, it does not modify the environment where the pO_2 is measured. EPR oximetry was previously used to monitor oxygenation in several types of tissues [18] such as brain [21–28], heart [29–34], gastrointestinal tract [35], skeletal muscle [36–38], liver [39–45], kidneys [46] and skin [47–49], to characterize the tumor microenvironment [50, 51], to measure oxygenation in ovarian grafts [52] and bone fractures [53–55]. Although EPR oximetry may be beneficial for studying the implication of oxygen during the healing process [56], to the best of our knowledge only 2 publications in the scientific literature have reported such application [57, 58]. To date, EPR oximetry has never been applied in the context of skin wound healing in diabetic models.

Therefore, the aim of this study was to assess the value of EPR oximetry to follow pO_2 variations during wound healing in diabetic models. For this purpose, we first validated the use of a murine diabetic model as an impaired wound healing model. Second, EPR oximetry was applied to two different types of wounds, a full-thickness excisional skin wound and a pedicled skin flap, and oxygenation was monitored during the healing process.

Materials and Methods

Two types of diabetic models were investigated: type 1 diabetes induced by streptozotocin (STZ) in NMRI mice and type 2 diabetes using genetically modified diabetic BKS(D)-Lepr^{db}/JOrIRj (db/db) mice. For non-diabetic controls, untreated NMRI mice or control db/+ mice were used. Two types of wound models were investigated: an excisional full-thickness skin wound and a pedicled skin flap. In each model, tissue oxygenation was monitored before and after surgery using lithium phthalocyanine (LiPc) crystals as oxygen sensor.

Animals

All animals used in this study were obtained from Elevage Janvier (France). Mice were housed individually in a temperature-controlled facility with a 12-hour dark/light cycle and received water and normal food ad libitum during all the experiment. All animal experiments were approved by the local Ethical Committee for animal care of the Université catholique de Louvain (authorization #2010/UCL/MD/01).

Diabetic models

Type 1 diabetes. Male 5 to 6-week-old NMRI mice received an intraperitoneal injection of 30 mg/kg of streptozotocin (STZ) (Sigma-Aldrich, Belgium) dissolved in citrate buffer (0.1 M, pH 4.5) during 5 consecutive days to induce a type 1 diabetes. The diabetic state was confirmed by measuring non-fasting blood glucose (NFBG) once a week until surgery. Blood was sampled

from the tail vein and analyzed with a GlucoMen LX Plus glucometer (Menarini Diagnostics, Italy). Animals were considered diabetic when NFBG was >250 mg/dL. Three groups of diabetic mice were included in the study: mice presenting NFBG >250 mg/dL for 4 weeks (STZ-4w), 5 weeks (STZ-5w) or 7 weeks (STZ-7w). For non-diabetic controls, untreated 9-week-old male NMRI mice were used.

Type 2 diabetes. Male BKS(D)-Lepr^{db}/JOrIRj (db/db) mice were used as a model of type 2 diabetes. These mice develop hyperphagia, obesity, hyperglycemia and hyperinsulinemia [59] due to an autosomal recessive mutation in the gene encoding the leptin receptor [60]. NFBG was controlled weekly (first measurement in 5-week-old mice) until surgery. Male age-matched control heterozygous littermates db/+ mice, that do not express the diabetic phenotype, were used as control non-diabetic mice.

Wound models

Full-thickness excisional skin wound model. The hair of the back of mice was shaved with an electric shaver before surgery. A full-thickness excisional skin wound was created on the dorsal midline with a 6 mm round skin biopsy punch (Kai Europe GmbH, Germany) during ketamine (80 mg/kg)/xylazine (8 mg/kg) anesthesia. A dressing was fixed on the wound with 6–0 sutures. Wound surgery was performed on STZ-treated diabetic mice, untreated non-diabetic NMRI mice, db/db mice and control db/+ mice.

Pedicled skin flap model. The hair of the back of mice was shaved prior to surgery. A U-shaped 30 x 8 mm pedicled skin flap was raised on the back of db/db mice and control db/+ mice during ketamine (80 mg/kg)/xylazine (8 mg/kg) anesthesia and stitched with 6–0 sutures. Pedicled flaps were made with a narrow pedicle (low ratio pedicle/length) to induce a hypoxic challenge at the distal part of the raised flap.

Kinetics of wound closure

Kinetics of closure of excisional full-thickness skin wounds were measured in healthy NMRI, STZ-4w, STZ-5w, STZ-7w, 12-week-old db/db and 12-week-old db/+ mice. Kinetics of closure were determined by measuring the wound diameter using a caliper during the healing process.

EPR oximetry

Implantation of LiPc crystals. Lithium phthalocyanine (LiPc) crystals, kindly provided by H.M. Swartz (Dartmouth Medical School, Hanover, NH, USA), were used as the oxygen-sensitive sensor [61]. They were placed in the tissue as follows:

Model 1—oxygen sensor in the center of excisional full-thickness wounds: LiPc crystals were placed with a 26 G needle in the center of the wounds, under the fascia, in untreated NMRI mice and 12-week-old db/db mice during wound surgery.

Model 2—oxygen sensor in the edges of excisional full-thickness wounds: After shaving of the back of 11-week-old db/db mice, LiPc crystals were placed in the healthy subcutaneous tissue using a 26 G needle under ketamine (80 mg/kg)/xylazine (8 mg/kg) anesthesia, 7 days before wound surgery.

Model 3—oxygen sensor in pedicled flaps: 7 to 10 days before wound surgery, the hair of the back of 11-week-old db/db and control db/+ mice was shaved and LiPc crystals were implanted subcutaneously using a 26 G needle under ketamine (80 mg/kg)/xylazine (8 mg/kg) anesthesia. LiPc crystals were placed on the dorsal midline at 2 sites separated by 10 mm in order to be at the proximal (15 mm from the pedicle) and distal (25 mm from the pedicle) parts of the raised flap.

EPR oximetry measurements. An EPR spectrometer (Magnettech, Berlin, Germany) equipped with a low-frequency microwave bridge operating at 1.2 GHz and an extended loop resonator (with 1-cm depth sensitivity) was used for pO_2 measurements. Animals under gaseous anesthesia (isoflurane, 2%), to preserve tissue oxygenation [62], were positioned in the EPR spectrometer, the region containing LiPc crystals placed under the surface coil. The temperature of mice was maintained to 37°C during measurements. Spectra were recorded with a modulation amplitude less than one third of the peak-to-peak line width. Parameters of acquisitions were the following: sweep field: 0.1 mT; sweep time: 20 to 30 s; number of points: 512–1024; number of scans: 5 to 20; modulation frequency: 10 kHz; modulation amplitude: 0.001875 to 0.00375 mT; power: 7.70–10.40 mW; gain: 200. The pO_2 of the tissue was determined by converting the peak-to-peak line width of the recorded EPR signal with a calibration determined previously for the same batch of LiPc crystals used in the present study (S1 Fig). Calibration was determined by flushing LiPc crystals at pO_2 ranged from 0 to 159.6 mmHg (0 to 21% O_2). Nitrogen and oxygen were mixed using an Aalborg gas mixer (Orangenburg, NY, USA) and the oxygen content was determined using a Servomex oxygen analyzer OA540 (Analytic Systems, Brussels, Belgium). EPR spectra were recorded using a Bruker EMX EPR spectrometer (Rheinstetten, Germany) operating at 9.5 GHz (X-band) and equipped with a temperature controller BVT-3000. Measurements were realized at 37°C. Parameters were the following: center field = 337.63 mT; sweep width = 0.3 mT; power = 0.1 mW; gain = 632; modulation frequency = 10 kHz; modulation amplitude = 0.001 mT; time constant = 5.12 ms; conversion time = 40.96 ms; sweep time = 20.97 s; 512 points; 3 scans.

The pO_2 was monitored repeatedly during the healing process. Control pO_2 values of healthy subcutaneous tissue were obtained by measuring repeatedly the pO_2 in unwounded non-diabetic and diabetic mice.

Response to pO_2 variations was verified one month after implantation of the oxygen sensor by a carbogen (95% O_2 and % CO_2) breathing challenge (hyperoxia) and after the animal sacrifice (acute hypoxia).

Intravital microscopy

Intravital microscopy was performed on db/+ and db/db mice as previously described [63]. Mice were shaved on the day before surgery. Animals were anesthetized with ketamine (80 mg/kg)/xylazine (8 mg/kg) and a two-sided titanium frame possessing a circular 12-mm opening was implanted on the dorsal skin flap of the mice. The opening was centered on a size-matched area where superficial skin and both the upper and lower fascia had been surgically removed. The titanium frame was sutured and the opening was closed with a circular glass coverslip secured with a snap ring. Fluorescein 5'-isothiocyanate (FITC) dextran (Sigma Aldrich, Belgium) was injected in the tail vein 10 minutes before imaging the skin microcirculation. Images were then captured using a CCD camera connected to an inverted Axiovert microscope (Zeiss, Germany).

Statistical analysis

Results were expressed as mean ± standard error of the mean (SEM).

One-way ANOVA followed by Dunnett's multiple comparison post hoc test or unpaired t-test was used to compare wound diameter between groups where appropriate.

For the comparison of pO_2 values at day 2 in excisional wounds *vs* basal pO_2 in unwounded tissue, unpaired t-test was used both for db/db and NMRI groups.

One-way ANOVA with Dunnett's multiple comparison post hoc test was used to compare wound pO_2 between groups in the flap model. P values <0.05 (*), <0.01 (**) and <0.001 (***)

were considered to be statistically significant. Statistical analyses were performed using GraphPad Prism 5 (GraphPad Software, La Jolla, CA, USA).

Results

Selection of diabetic animal model

Two types of diabetes were investigated to evaluate if diabetes induces impaired healing in mouse models. Non-fasting blood glucose (NFBG) was monitored to verify the diabetic state. When diabetes was verified, kinetics of wound closure were monitored to evaluate if diabetic models presented impaired wound healing.

Non-fasting blood glucose. Non-fasting blood glucose (NFBG) was monitored weekly in STZ-induced and db/db mice to confirm the diabetic state before wounding. In the STZ-induced diabetic group, NFBG was 168 ± 8 mg/dL prior to STZ treatment. Mice injected with STZ became hyperglycemic (NFBG > 250 mg/dL) 5 to 12 days after the last STZ injection. Then, NFBG remained above 250 mg/dL until excisional full-thickness skin wounding was performed 4 (STZ-4w), 5 (STZ-5w) or 7 weeks (STZ-7w) later (Fig 1). At the time of wounding, NFBG was 556 ± 42 mg/dL, 536 ± 24 mg/dL and 457 ± 27 mg/dL, respectively, for STZ-4w, STZ-5w and STZ-7w mice. Db/db mice had a NFBG above 250 mg/dL during the 7-week follow-up before wounding. At the time of surgery, 12-week-old db/db mice had a NFBG of 504 ± 45 mg/dL. Non-diabetic control db/+ mice had a NFBG of 120 ± 16 mg/dL at wounding time.

Diabetes was thus confirmed in all diabetic mouse models at the time of surgery.

Wound closure kinetics in the different diabetic models. In order to determine which type of diabetic murine model was the most relevant for this study, the kinetics of closure of excisional full-thickness skin wounds were quantified in the different models by measuring the wound diameter during the healing process. No difference was observed in the kinetics of closure of excisional full-thickness skin wounds in the STZ-4w, STZ-5w and STZ-7w groups compared to the control non-diabetic group (Fig 2a). In contrast, complete wound closure was highly significantly delayed in db/db mice (full closure at 35 days) compared to db/+ mice (full closure at 18 days) (Fig 2b).

At day 14, no significant difference was observed in the wound size between STZ-4w, STZ-5w, STZ-7w and control non-diabetic mice (Fig 3a), whereas the wound size was significantly larger in db/db compared to db/+ mice (6.28 ± 0.31 mm *vs* 2.72 ± 0.50 mm; $p < 0.001$) (Fig 3b). Consequently, db/db mice were selected as the model of impaired wound healing for the oxygenation study.

EPR oximetry

Basal pO_2 values in the unwounded subcutaneous tissue. In the unwounded subcutaneous tissue, a mean pO_2 value of 18.8 ± 1.2 mmHg was measured in non-diabetic NMRI mice. In diabetic mice, the mean pO_2 value was 20.7 ± 1.2 mmHg. No significant difference was observed between the basal pO_2 in non-diabetic and diabetic mice (unpaired t test, $p = 0.31$). The pO_2 was stable during a 1-month monitoring period.

Also, we observed that the response to pO_2 variations was preserved one month after LiPc implantation (Fig 4).

Model 1: oxygen sensor in the center of excisional full-thickness wounds. In the center of excisional full-thickness skin wounds (Fig 5b and 5c), high pO_2 values were observed at day 2 similarly in diabetic (40.8 ± 9.2 mmHg) and control non-diabetic (48.4 ± 5.6 mmHg) mice. These values were significantly higher than those measured in the unwounded subcutaneous tissue in both diabetic (20.7 ± 1.2 mmHg, $p = 0.012$, unpaired t-test) and non-diabetic

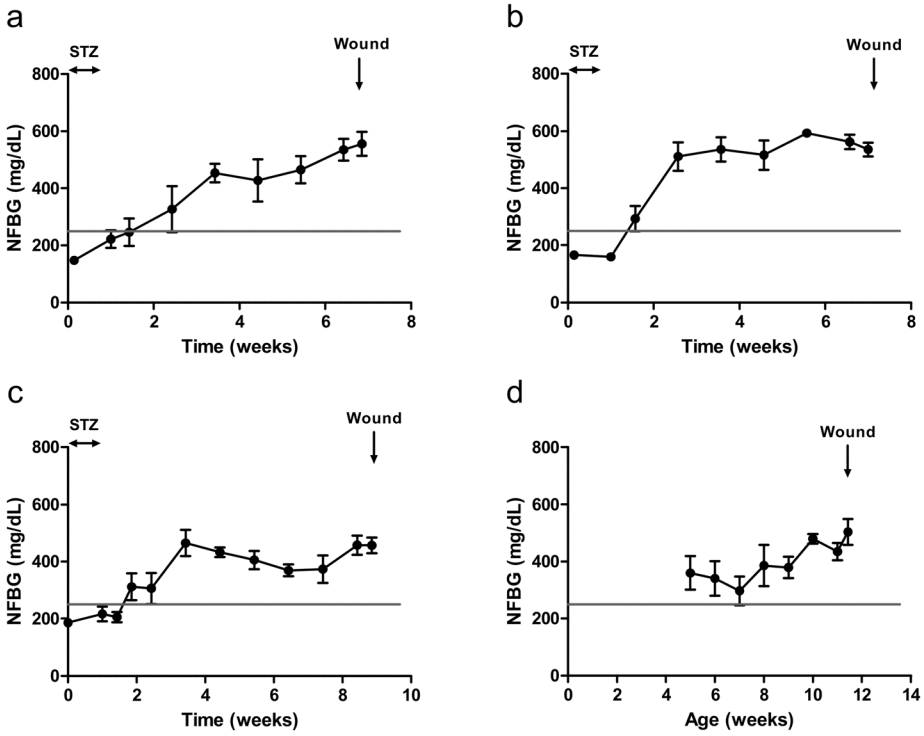

Fig 1. Confirmation of diabetic state before wounding. NFBG was monitored weekly in STZ-induced diabetes after 4 weeks (a), 5 weeks (b) and 7 weeks (c) and in genetically modified db/db mice (d). Mice were considered to be diabetic when NFBG >250 mg/dL. Results are expressed as mean ± SEM (n = 4).

doi:10.1371/journal.pone.0144914.g001

(18.8 ± 1.2 mmHg, p = 0.009, unpaired t-test) mice. In this configuration, the oxygen sensor located at the center of wounds was in direct contact with surrounding air. After 7 days, the pO_2 decreased regularly to reach values normally observed in the healthy subcutaneous tissue (Fig 5a). At this time, the LiPc sensor was trapped in the neo-formed granulation tissue of wounds.

Model 2: oxygen sensor in the edges of excisional full-thickness wounds. With sensors at the edges of excisional wounds (Fig 6b and 6c), basal pO_2 value 1 day prior to surgery was 24.7 ± 2.1 mmHg consistent with values obtained in the subcutaneous healthy tissue. A pO_2

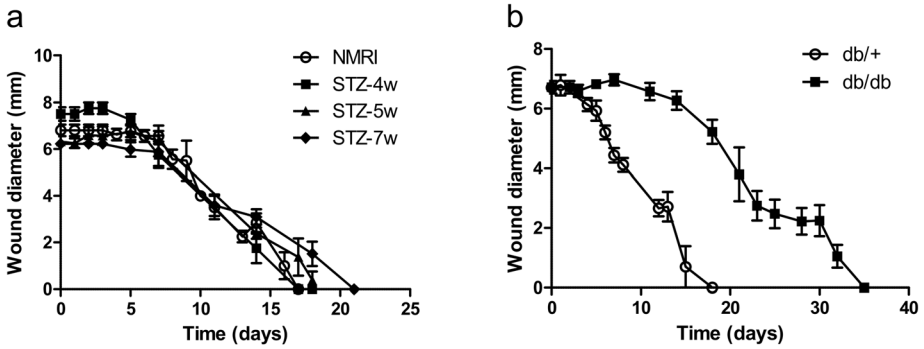

Fig 2. Db/db mice exhibit delayed excisional wound closure. Kinetics of wound closure were monitored in STZ-induced diabetic mice *vs* control NMRI mice (a) and db/db mice *vs* control db/+ mice (b). Results are expressed as mean ± SEM (n = 4–6).

doi:10.1371/journal.pone.0144914.g002

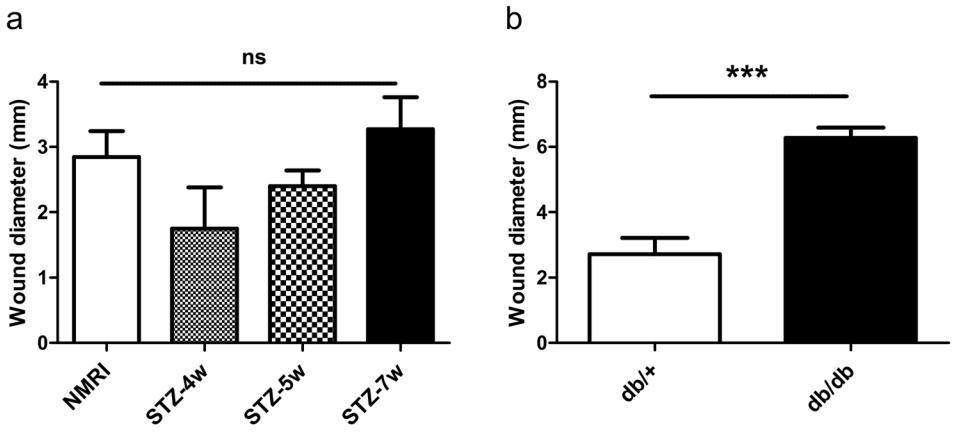

Fig 3. Db/db mice exhibit impaired wound healing. Wound diameter at day 14 in STZ-induced diabetic mice *vs* control NMRI mice (a) and db/db mice *vs* control db/+ mice (b). Results are expressed as mean ± SEM (n = 4–6). ns: non significant (One-way ANOVA and Dunnett's multiple comparison post hoc test, comparison with control NMRI mice); ***: p<0.001 (unpaired t-test).

doi:10.1371/journal.pone.0144914.g003

increase was observed from day 1 to day 3. At day 15, pO_2 was decreased to recover normal basal values (Fig 6a).

Model 3: oxygen sensor in pedicled skin flaps. In the flap model, LiPc crystals were implanted both at the proximal and distal region of the flaps (Fig 7b).

Basal pO_2 values recorded before surgery were similar in db/db (proximal site: 18.4 ± 1.3 mmHg / distal site: 18.3 ± 1.1 mmHg) and db/+ (proximal site: 20.0 ± 0.6 mmHg / distal site: 17.7 ± 0.7 mmHg) mice, and consistent with pO_2 values measured in the unwounded subcutaneous tissue in db/db (20.7 ± 1.2 mmHg) and in non-diabetic (18.8 ± 1.2 mmHg) mice (Fig 7a). One day after surgery, a drop in pO_2 was observed in the 2 regions of the flaps in both diabetic (proximal site: 9.4 ± 0.2 mmHg / distal site: 10.5 ± 0.3 mmHg) and non-diabetic (proximal site: 8.8 ± 0.5 mmHg / distal site: 9.2 ± 0.6 mmHg) mice. In diabetic mice, the pO_2

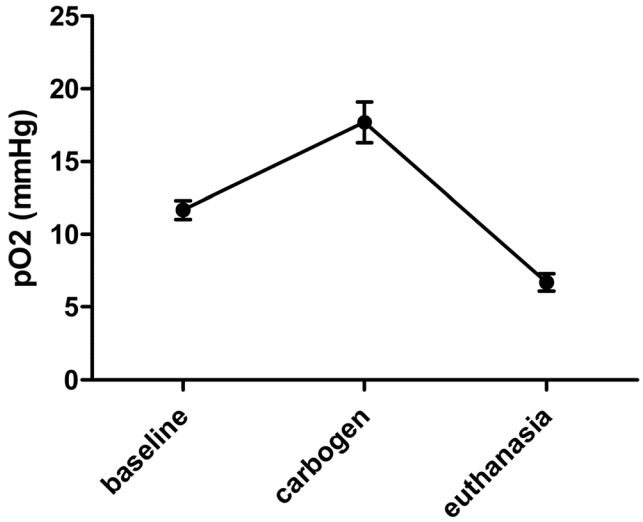

Fig 4. LiPc crystals responded to pO_2 variations one month after the implantation in the skin tissue. Typical experiment realized on a mouse 1 month after implantation of the LiPc crystals in the tissue. Results are expressed as mean ± SEM (n = 3–4).

doi:10.1371/journal.pone.0144914.g004

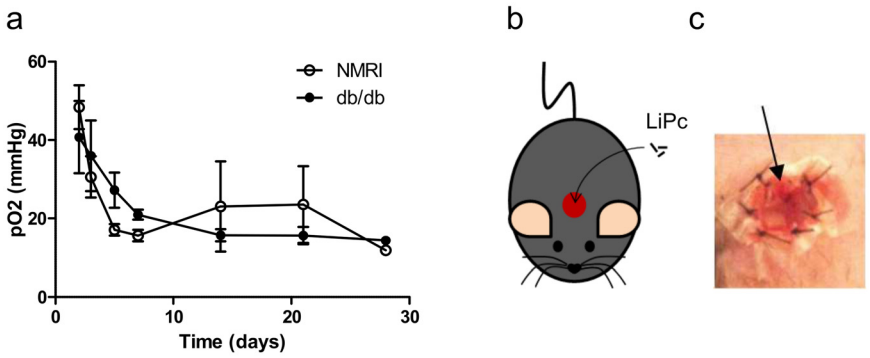

Fig 5. High pO_2 is observed at the center of full-thickness excisional skin wounds early after wounding. LiPc crystals were implanted at the center of excisional wounds in control NMRI and diabetic db/db mice during the surgery (b, c) and pO_2 was monitored repeatedly by EPR oximetry during wound healing. Results are expressed as mean ± SEM (n = 4) (a).

doi:10.1371/journal.pone.0144914.g005

remained low at proximal and distal sites until the end of the monitoring (10.0 ± 0.4 mmHg and 10.9 ± 0.3 mmHg at day 3, 14.0 ± 0.9 mmHg and 15.2 ± 1.7 mmHg at day 7, 10.5 ± 1.6 mmHg and 10.3 ± 1.9 mmHg at day 11). Macroscopically, diabetic flaps were necrotic on a large area (Fig 7c). On the contrary, in non-diabetic mice, the pO_2 increased to reach values of 12.2 ± 1.3 mmHg and 14.9 ± 1.7 mmHg at day 3, 21.3 ± 2.0 mmHg and 17.4 ± 2.7 mmHg at day 7 for the proximal and distal regions, respectively. Macroscopically, flaps in non-diabetic mice healed with only little or no necrosis (Fig 7c).

Intravital microscopy—microangiopathies

Microangiopathies were evaluated by intravital microscopy. In the non-diabetic skin (Fig 8, left), a well-organized microvasculature was observed. In the diabetic skin, the microvascular network was disorganized and fewer vessels were observed compared to the non-diabetic skin (Fig 8, right). Moreover, in diabetic mice, hemorrhages were observed at the extremity of some vessels.

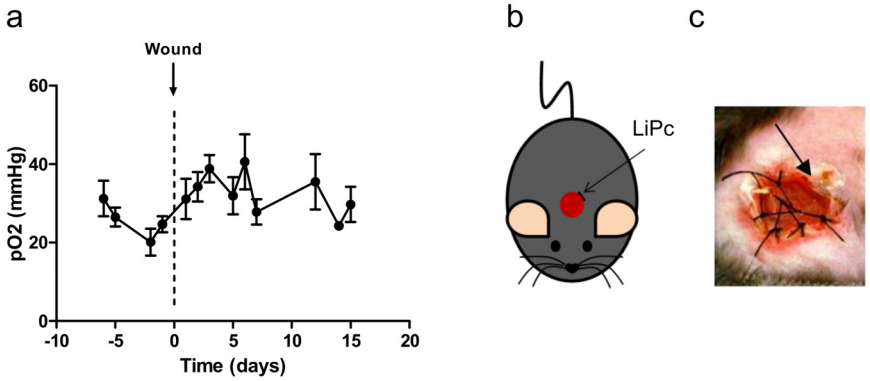

Fig 6. The periphery of full-thickness excisional skin wounds does not exhibit hypoxia. LiPc crystals were implanted 7 days prior to surgery at the periphery of diabetic excisional wounds (db/db mice) (b, c) and pO_2 was monitored repeatedly by EPR oximetry during wound healing. Results are expressed as mean ± SEM (n = 4) (a).

doi:10.1371/journal.pone.0144914.g006

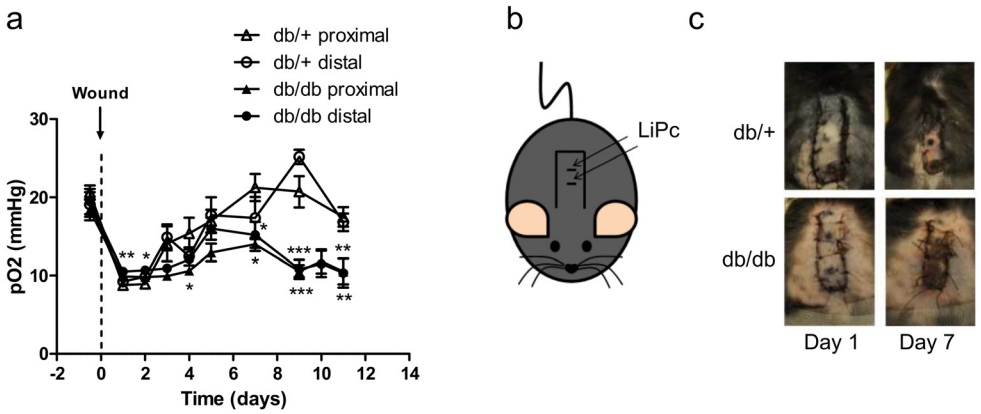

Fig 7. Pedicled skin flaps exhibit prolonged hypoxia in diabetic db/db mice contrarily to control db/+ mice. LiPc was implanted in the back of diabetic db/db (n = 14) and non-diabetic db/+ mice (n = 12) (b, c) 7 to 10 days prior to surgery. The pO_2 measurements by EPR oximetry were realized at distal and proximal regions of the flaps. Results are expressed as mean ± SEM (a). *: p <0.05, **: p<0.01 and ***: p<0.001 (One-way ANOVA and Dunnett's Multiple Comparison post hoc test, comparison with db/+ proximal).

doi:10.1371/journal.pone.0144914.g007

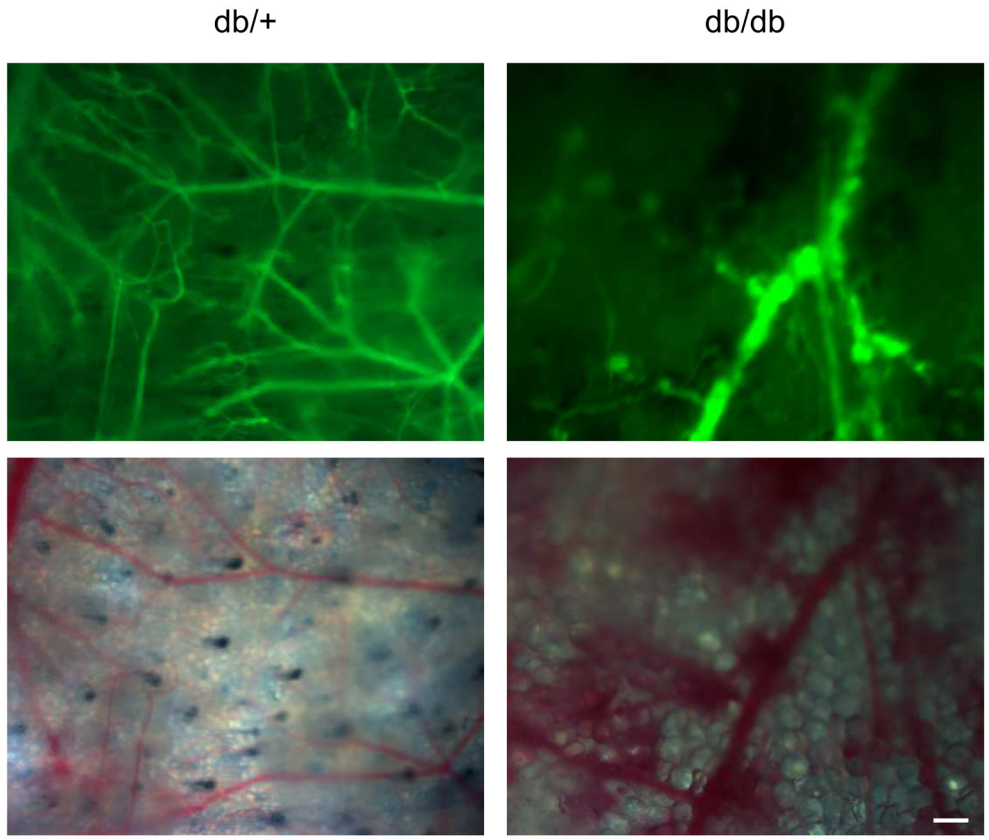

Fig 8. Db/db mice exhibit microvascular defects. Skin microvascular network was observed by intravital microscopy in db/+ (left) and db/db (right) mice. Images were acquired 10 minutes after a FITC-dextran injection in the tail vein. Top: fluorescence images, bottom: visible light images (scale bar = 200 μm).

doi:10.1371/journal.pone.0144914.g008

Discussion

Despite the important role of oxygen in wound healing, wound oxygenation measurement is still challenging. EPR oximetry is a technique that allows absolute pO_2 measurements that can be repeated at the same site over long periods of time, up to at least 5 years [20]. However, to date, it has never been used in the particular context of wound healing in diabetic models. This was the purpose of the present study. We showed that LiPc crystals, used as the oxygen sensor, allowed repeated and reliable pO_2 measurements in the normal subcutaneous tissue. Indeed, the stability of the pO_2 measurements using this oxygen sensor was verified in normal conditions, in the unwounded subcutaneous tissue. Also, a good response to hyperoxic and hypoxic challenges was observed 1 month after implantation in the subcutaneous tissue. The pertinence of wound pO_2 measurements by EPR oximetry was determined using 2 wound models, a full-thickness excisional skin wound and a pedicled skin flap, in type 2 genetically induced diabetic db/db mice in which we observed impaired wound healing, in accordance with the literature [64–66]. In the flap model, reliable longitudinal pO_2 measurements were obtained during the wound healing process. First, as expected, an important and sharp decrease in pO_2 was observed one day after wounding. Indeed, in this model, the oxygen supply is dramatically decreased at the distal part of the flap as it depends only on the base of the pedicle, whereas vessels coming from the other sides are disrupted by the surgical incision and dissection [67]. Interestingly, the pO_2 variations measured during the healing process were correlated with the macroscopic aspect of the lesion. In diabetic db/db mice, consistent with the massive necrosis observed in all animals at 7 days post wounding and microvascular defects (decrease in vessels density, unorganized vascular network, and hemorrhages observed by intravital microscopy), sustained hypoxia was evident during the entire pO_2 monitoring period. In comparison, we observed a progressive reoxygenation of the flap linked to complete recovery in non-diabetic control db/+ mice. In the other wound model that was investigated, excisional wounds, positioning the oxygen sensor appropriately was more challenging. Contrary to the flap in which the oxygen sensor was inserted in the skin tissue undergoing flap surgery, excisional wounds are characterized by a complete removal of the wounded skin tissue. The oxygen sensor was consequently placed under the remaining thin fascia in the wound bed. When the oxygen sensor was located at the center of excisional wounds, in the wound bed, we observed significantly high pO_2 values early after wounding that were not in agreement with the hypoxic state classically described at the early stage of wound healing [5]. Indeed, the disruption of blood vessels induced by wounding normally restricts oxygen supply to the wounded site and the increased metabolic activity of cells implicated in wound healing leads to an increase in oxygen consumption rate [5]. But it appeared that placing the oxygen sensor at this superficial position in the wound led to an over-estimation of the pO_2 due to the influence of the surrounding atmospheric air on pO_2 measurements, even if the sensor was laid under the fascia and the wound covered by a dressing. Placing LiPc crystals in the skin tissue at the edges of excisional wounds limited the influence of atmospheric oxygen. Indeed, in the skin tissue, we didn't observe any difference in pO_2 measurements when varying the oxygen concentration (0, 21 and 95%) in the surrounding atmosphere (data not shown). However, after wounding, we did not observe periods of hypoxia in this open wound model. Consequently, to reproduce hypoxia episodes, pedicled skin flap models are more appropriate.

A limitation linked to the EPR measurements is inherent to the size of LiPc crystals used in the study that was rather large compared to the mouse skin thickness. The length of the crystals was about hundreds of μm to 1 mm, limiting somewhat spatial measurement accuracy. It was in fact impossible to differentiate pO_2 values in the different parts of the mouse skin (dermis

and epidermis) and it allowed only determining a mean pO_2 value at the implantation site in a volume of approximately 0.1 to 1 mm^3.

Also, in order to increase the sensitivity of measurements, several crystals were implanted in the tissue. The sensor response to oxygen was not affected by the use of several crystals. Nevertheless, as measurements reflect the mean pO_2 at the implantation site, the spatial accuracy will be lower when several crystals are used, instead of a single one, but only if a spatial dispersion of the crystals has occurred.

It must also be pointed out that the form of LiPc crystals is an important factor, as oxygen sensitivity is dependent on the structure of the crystal [68, 69]. In this study, we carefully implanted LiPc in the tissue in order not to break crystals and avoided the implantation of LiPc as a crushed powder. The aspect of LiPc crystals was verified at the end of the experiment, and the integrity of the sensors was confirmed.

Apart from the limitations attributed to the wound model and the oxygen sensor, it appeared that the choice of the animal model presenting wound healing impairment was not so straightforward. Contrary to the db/db mouse model, we did not observe any significant healing impairment in the STZ-induced diabetic mice tested. This was quite surprising as the type 1 STZ-induced diabetic model is classically used in impaired wound healing studies [70]. To allow mice to develop chronic complications of diabetes like microangiopathies, a delay of 4, 5 and 7 weeks was allowed between the occurrence of the diabetic state (confirmed by glycaemia measurements) and the wound surgery. This is the range classically mentioned in wound healing studies using this model [71, 72]. Nevertheless, even 7 weeks after the occurrence of the diabetic state, only a slight effect of diabetes was observed on wound healing kinetics. A significant effect should have been observed when the latency time between the occurrence of diabetes and wounding was longer than 7 weeks (for instance 8 to 12 weeks). An even longer delay was not tested for logistical reasons. So, the STZ-induced diabetic mice were excluded from the study and the db/db mice were selected for the wound oximetry study.

In conclusion, this study established that EPR oximetry using LiPc crystals as the oxygen sensor is applicable to monitor tissue pO_2 during wound healing in acute and chronic wounds, in normal and diabetic animals. Nonetheless, the technique is limited for measurements in a skin flap and cannot be applied to excisional wounds in which diffusion of atmospheric oxygen significantly affects the measurements. Using the flap model, this technique could be used to evaluate the effects of pharmacological treatments on wound oxygenation and healing.

Supporting Information

S1 Fig. PO_2 calibration curve performed with LiPc crystals. Line width (LW) in Gauss (G) of the EPR spectrum in function of the pO_2. Results are expressed as mean ± standard deviation (n = 5).
(TIF)

Author Contributions

Conceived and designed the experiments: CMD DD PL BG. Performed the experiments: CMD AL SV PEP PL. Analyzed the data: CMD AL SV PEP PS DD PL BG. Contributed reagents/materials/analysis tools: CMD AL SV PEP PS DD PL BG. Wrote the paper: CMD AL SV PEP PS DD PL BG.

References

1. Gurtner GC, Werner S, Barrandon Y, Longaker MT. Wound repair and regeneration. Nature. 2008; 453 (7193):314–21. doi: 10.1038/nature07039 PMID: 18480812

2. Singer AJ, Clark RA. Cutaneous wound healing. N Engl J Med. 1999; 341(10):738–46. PMID: 10471461
3. Lazarus GS, Cooper DM, Knighton DR, Percoraro RE, Rodeheaver G, Robson MC. Definitions and guidelines for assessment of wounds and evaluation of healing. Wound Repair Regen. 1994; 2(3):165–70. PMID: 17156107
4. Mustoe TA, O'Shaughnessy K, Kloeters O. Chronic wound pathogenesis and current treatment strategies: a unifying hypothesis. Plast Reconstr Surg. 2006; 117(7 Suppl):35S–41S. PMID: 16799373
5. Tandara AA, Mustoe TA. Oxygen in wound healing—more than a nutrient. World J Surg. 2004; 28 (3):294–300. PMID: 14961188
6. Schreml S, Szeimies RM, Prantl L, Karrer S, Landthaler M, Babilas P. Oxygen in acute and chronic wound healing. Br J Dermatol. 2010; 163(2):257–68. doi: 10.1111/j.1365-2133.2010.09804.x PMID: 20394633
7. Gordillo GM, Sen CK. Revisiting the essential role of oxygen in wound healing. Am J Surg. 2003; 186 (3):259–63. PMID: 12946829
8. Allen DB, Maguire JJ, Mahdavian M, Wicke C, Marcocci L, Scheuenstuhl H, et al. Wound hypoxia and acidosis limit neutrophil bacterial killing mechanisms. Arch Surg. 1997; 132(9):991–6. PMID: 9301612
9. Prockop DJ, Kivirikko KI, Tuderman L, Guzman NA. The biosynthesis of collagen and its disorders (first of two parts). N Engl J Med. 1979; 301(1):13–23. PMID: 449904
10. Hopf HW. Development of subcutaneous wound oxygen measurement in humans: contributions of Thomas K Hunt, MD. Wound Repair Regen. 2003; 11(6):424–30. PMID: 14617281
11. Hunt TK, Twomey P, Zederfeldt B, Dunphy JE. Respiratory gas tensions and pH in healing wounds. Am J Surg. 1967; 114(2):302–7. PMID: 6028994
12. Niinikoski J, Grislis G, Hunt TK. Respiratory gas tensions and collagen in infected wounds. Ann Surg. 1972; 175(4):588–93. PMID: 4553582
13. Schreml S, Meier RJ, Wolfbeis OS, Maisch T, Szeimies RM, Landthaler M, et al. 2D luminescence imaging of physiological wound oxygenation. Exp Dermatol. 2011; 20(7):550–4. doi: 10.1111/j.1600-0625.2011.01263.x PMID: 21443617
14. Schreml S, Meier RJ, Kirschbaum M, Kong SC, Gehmert S, Felthaus O, et al. Luminescent dual sensors reveal extracellular pH-gradients and hypoxia on chronic wounds that disrupt epidermal repair. Theranostics. 2014; 4(7):721–35. doi: 10.7150/thno.9052 PMID: 24883122
15. Li Z, Roussakis E, Koolen PG, Ibrahim AM, Kim K, Rose LF, et al. Non-invasive transdermal two-dimensional mapping of cutaneous oxygenation with a rapid-drying liquid bandage. Biomed Opt Express. 2014; 5(11):3748–64. doi: 10.1364/BOE.5.003748 PMID: 25426308
16. Dunn JF, Swartz HM. In vivo electron paramagnetic resonance oximetry with particulate materials. Methods. 2003; 30(2):159–66. PMID: 12725782
17. Khan N, Williams BB, Hou H, Li H, Swartz HM. Repetitive tissue pO2 measurements by electron paramagnetic resonance oximetry: current status and future potential for experimental and clinical studies. Antioxid Redox Signal. 2007; 9(8):1169–82. PMID: 17536960
18. Gallez B, Baudelet C, Jordan BF. Assessment of tumor oxygenation by electron paramagnetic resonance: principles and applications. NMR Biomed. 2004; 17(5):240–62. PMID: 15366026
19. Ahmad R, Kuppusamy P. Theory, instrumentation, and applications of electron paramagnetic resonance oximetry. Chem Rev. 2010; 110(5):3212–36. doi: 10.1021/cr900396q PMID: 20218670
20. Swartz HM, Williams BB, Zaki BI, Hartford AC, Jarvis LA, Chen EY, et al. Clinical EPR: unique opportunities and some challenges. Acad Radiol. 2014; 21(2):197–206. doi: 10.1016/j.acra.2013.10.011 PMID: 24439333
21. Rolett EL, Azzawi A, Liu KJ, Yongbi MN, Swartz HM, Dunn JF. Critical oxygen tension in rat brain: a combined (31)P-NMR and EPR oximetry study. Am J Physiol Regul Integr Comp Physiol. 2000; 279 (1):R9–R16. PMID: 10896858
22. Dunn JF, O'Hara JA, Zaim-Wadghiri Y, Lei H, Meyerand ME, Grinberg OY, et al. Changes in oxygenation of intracranial tumors with carbogen: a BOLD MRI and EPR oximetry study. J Magn Reson Imaging. 2002; 16(5):511–21. PMID: 12412027
23. Lei H, Grinberg O, Nwaigwe CI, Hou HG, Williams H, Swartz HM, et al. The effects of ketamine-xylazine anesthesia on cerebral blood flow and oxygenation observed using nuclear magnetic resonance perfusion imaging and electron paramagnetic resonance oximetry. Brain Res. 2001; 913(2):174–9. PMID: 11549383
24. Hou H, Grinberg OY, Taie S, Leichtweis S, Miyake M, Grinberg S, et al. Electron paramagnetic resonance assessment of brain tissue oxygen tension in anesthetized rats. Anesth Analg. 2003; 96 (5):1467–72, table of contents. PMID: 12707151

25. Liu S, Timmins GS, Shi H, Gasparovic CM, Liu KJ. Application of in vivo EPR in brain research: monitoring tissue oxygenation, blood flow, and oxidative stress. NMR Biomed. 2004; 17(5):327–34. PMID: 15366032

26. O'Hara JA, Khan N, Hou H, Wilmo CM, Demidenko E, Dunn JF, et al. Comparison of EPR oximetry and Eppendorf polarographic electrode assessments of rat brain PtO2. Physiol Meas. 2004; 25(6):1413–23. PMID: 15712720

27. Weaver J, Jalal FY, Yang Y, Thompson J, Rosenberg GA, Liu KJ. Tissue oxygen is reduced in white matter of spontaneously hypertensive-stroke prone rats: a longitudinal study with electron paramagnetic resonance. J Cereb Blood Flow Metab. 2014; 34(5):890–6. doi: 10.1038/jcbfm.2014.35 PMID: 24549186

28. Weaver J, Yang Y, Purvis R, Weatherwax T, Rosen GM, Liu KJ. In vivo evidence of methamphetamine induced attenuation of brain tissue oxygenation as measured by EPR oximetry. Toxicol Appl Pharmacol. 2014; 275(2):73–8. doi: 10.1016/j.taap.2013.12.023 PMID: 24412707

29. Zweier JL, Thompson-Gorman S, Kuppusamy P. Measurement of oxygen concentrations in the intact beating heart using electron paramagnetic resonance spectroscopy: a technique for measuring oxygen concentrations in situ. J Bioenerg Biomembr. 1991; 23(6):855–71. PMID: 1663949

30. Kuppusamy P, Chzhan M, Vij K, Shteynbuk M, Lefer DJ, Giannella E, et al. Three-dimensional spectral-spatial EPR imaging of free radicals in the heart: a technique for imaging tissue metabolism and oxygenation. Proc Natl Acad Sci U S A. 1994; 91(8):3388–92. PMID: 8159757

31. Friedman BJ, Grinberg OY, Isaacs KA, Ruuge EK, Swartz HM. Effect of repetitive ischemia on myocardial oxygen tension in isolated perfused and hypoperfused rat hearts. Magn Reson Med. 1996; 35 (2):214–20. PMID: 8622586

32. Grinberg OY, Friedman BJ, Swartz HM. Intramyocardial pO2 measured by EPR. Adv Exp Med Biol. 1997; 428:261–8. PMID: 9500056

33. Grinberg OY, Grinberg SA, Friedman BJ, Swartz HM. Myocardial oxygen tension and capillary density in the isolated perfused rat heart during pharmacological intervention. Adv Exp Med Biol. 1997; 411:171–81. PMID: 9269425

34. Khan M, Kwiatkowski P, Rivera BK, Kuppusamy P. Oxygen and oxygenation in stem-cell therapy for myocardial infarction. Life Sci. 2010; 87(9–10):269–74. doi: 10.1016/j.lfs.2010.06.013 PMID: 20600148

35. He G, Shankar RA, Chzhan M, Samouilov A, Kuppusamy P, Zweier JL. Noninvasive measurement of anatomic structure and intraluminal oxygenation in the gastrointestinal tract of living mice with spatial and spectral EPR imaging. Proc Natl Acad Sci U S A. 1999; 96(8):4586–91. PMID: 10200306

36. Grinberg OY, Hou H, Grinberg SA, Moodie KL, Demidenko E, Friedman BJ, et al. pO2 and regional blood flow in a rabbit model of limb ischemia. Physiol Meas. 2004; 25(3):659–70. PMID: 15253117

37. Helisch A, Wagner S, Khan N, Drinane M, Wolfram S, Heil M, et al. Impact of mouse strain differences in innate hindlimb collateral vasculature. Arterioscler Thromb Vasc Biol. 2006; 26(3):520–6. PMID: 16397137

38. Matsumoto A, Matsumoto S, Sowers AL, Koscielniak JW, Trigg NJ, Kuppusamy P, et al. Absolute oxygen tension (pO(2)) in murine fatty and muscle tissue as determined by EPR. Magn Reson Med. 2005; 54(6):1530–5. PMID: 16276490

39. Nakashima T, Goda F, Jiang J, Shima T, Swartz HM. Use of EPR oximetry with India ink to measure the pO2 in the liver in vivo in mice. Magn Reson Med. 1995; 34(6):888–92. PMID: 8598816

40. Jiang J, Nakashima T, Liu KJ, Goda F, Shima T, Swartz HM. Measurement of PO2 in liver using EPR oximetry. J Appl Physiol (1985). 1996; 80(2):552–8.

41. Gallez B, Debuyst R, Dejehet F, Liu KJ, Walczak T, Goda F, et al. Small particles of fusinite and carbohydrate chars coated with aqueous soluble polymers: preparation and applications for in vivo EPR oximetry. Magn Reson Med. 1998; 40(1):152–9. PMID: 9660565

42. James PE, Miyake M, Swartz HM. Simultaneous measurement of NO(*) and PO(2) from tissue by in vivo EPR. Nitric Oxide. 1999; 3(4):292–301. PMID: 10444368

43. James PE, Madhani M, Roebuck W, Jackson SK, Swartz HM. Endotoxin-induced liver hypoxia: defective oxygen delivery versus oxygen consumption. Nitric Oxide. 2002; 6(1):18–28. PMID: 11829531

44. Madhani M, Barchowsky A, Klei L, Ross CR, Jackson SK, Swartz HM, et al. Antibacterial peptide PR-39 affects local nitric oxide and preserves tissue oxygenation in the liver during septic shock. Biochim Biophys Acta. 2002; 1588(3):232–40. PMID: 12393178

45. Towner RA, Sturgeon SA, Khan N, Hou H, Swartz HM. In vivo assessment of nodularin-induced hepatotoxicity in the rat using magnetic resonance techniques (MRI, MRS and EPR oximetry). Chem Biol Interact. 2002; 139(3):231–50. PMID: 11879814

46. James PE, Bacic G, Grinberg OY, Goda F, Dunn JF, Jackson SK, et al. Endotoxin-induced changes in intrarenal pO2, measured by in vivo electron paramagnetic resonance oximetry and magnetic resonance imaging. Free Radic Biol Med. 1996; 21(1):25–34. PMID: 8791090

47. Krzic M, Sentjurc M, Kristl J. Improved skin oxygenation after benzyl nicotinate application in different carriers as measured by EPR oximetry in vivo. J Control Release. 2001; 70(1–2):203–11. PMID: 11166420

48. Abramovic Z, Sentjurc M, Kristl J, Khan N, Hou H, Swartz HM. Influence of different anesthetics on skin oxygenation studied by electron paramagnetic resonance in vivo. Skin Pharmacol Physiol. 2007; 20 (2):77–84. PMID: 17143012

49. Abramovic Z, Sustarsic U, Teskac K, Sentjurc M, Kristl J. Influence of nanosized delivery systems with benzyl nicotinate and penetration enhancers on skin oxygenation. Int J Pharm. 2008; 359(1–2):220–7. doi: 10.1016/j.ijpharm.2008.03.014 PMID: 18472233

50. Gallez B, Jordan BF, Baudelet C, Misson PD. Pharmacological modifications of the partial pressure of oxygen in murine tumors: evaluation using in vivo EPR oximetry. Magn Reson Med. 1999; 42(4):627–30. PMID: 10502749

51. Hou H, Abramovic Z, Lariviere JP, Sentjurc M, Swartz H, Khan N. Effect of a topical vasodilator on tumor hypoxia and tumor oxygen guided radiotherapy using EPR oximetry. Radiat Res. 2010; 173 (5):651–8. doi: 10.1667/RR1947.1 PMID: 20426665

52. Van Eyck AS, Jordan BF, Gallez B, Heilier JF, Van Langendonckt A, Donnez J. Electron paramagnetic resonance as a tool to evaluate human ovarian tissue reoxygenation after xenografting. Fertil Steril. 2009; 92(1):374–81. doi: 10.1016/j.fertnstert.2008.05.012 PMID: 18692811

53. Lu C, Rollins M, Hou H, Swartz HM, Hopf H, Miclau T, et al. Tibial fracture decreases oxygen levels at the site of injury. Iowa Orthop J. 2008; 28:14–21. PMID: 19223943

54. Lu C, Saless N, Hu D, Wang X, Xing Z, Hou H, et al. Mechanical stability affects angiogenesis during early fracture healing. J Orthop Trauma. 2011; 25(8):494–9. PMID: 21738063

55. Lu C, Saless N, Wang X, Sinha A, Decker S, Kazakia G, et al. The role of oxygen during fracture healing. Bone. 2013; 52(1):220–9. doi: 10.1016/j.bone.2012.09.037 PMID: 23063782

56. Parinandi NL, Sen CK, Kuppusamy P. Joint International Conference on EPR Spectroscopy and wound healing. Antioxid Redox Signal. 2006; 8(7–8):1385–7. PMID: 16910786

57. Biswas S, Roy S, Banerjee J, Hussain SR, Khanna S, Meenakshisundaram G, et al. Hypoxia inducible microRNA 210 attenuates keratinocyte proliferation and impairs closure in a murine model of ischemic wounds. Proc Natl Acad Sci U S A. 2010; 107(15):6976–81. doi: 10.1073/pnas.1001653107 PMID: 20308562

58. Isenberg JS, Hyodo F, Matsumoto K, Romeo MJ, Abu-Asab M, Tsokos M, et al. Thrombospondin-1 limits ischemic tissue survival by inhibiting nitric oxide-mediated vascular smooth muscle relaxation. Blood. 2007; 109(5):1945–52. PMID: 17082319

59. Coleman DL. Obese and diabetes: two mutant genes causing diabetes-obesity syndromes in mice. Diabetologia. 1978; 14(3):141–8. PMID: 350680

60. Chen H, Charlat O, Tartaglia LA, Woolf EA, Weng X, Ellis SJ, et al. Evidence that the diabetes gene encodes the leptin receptor: identification of a mutation in the leptin receptor gene in db/db mice. Cell. 1996; 84(3):491–5. PMID: 8608603

61. Liu KJ, Gast P, Moussavi M, Norby SW, Vahidi N, Walczak T, et al. Lithium phthalocyanine: a probe for electron paramagnetic resonance oximetry in viable biological systems. Proc Natl Acad Sci U S A. 1993; 90(12):5438–42. PMID: 8390665

62. Baudelet C, Gallez B. Effect of anesthesia on the signal intensity in tumors using BOLD-MRI: comparison with flow measurements by Laser Doppler flowmetry and oxygen measurements by luminescence-based probes. Magn Reson Imaging. 2004; 22(7):905–12. PMID: 15288130

63. Porporato PE, Payen VL, De Saedeleer CJ, Preat V, Thissen JP, Feron O, et al. Lactate stimulates angiogenesis and accelerates the healing of superficial and ischemic wounds in mice. Angiogenesis. 2012; 15(4):581–92. doi: 10.1007/s10456-012-9282-0 PMID: 22660894

64. Michaels Jt, Churgin SS, Blechman KM, Greives MR, Aarabi S, Galiano RD, et al. db/db mice exhibit severe wound-healing impairments compared with other murine diabetic strains in a silicone-splinted excisional wound model. Wound Repair Regen. 2007; 15(5):665–70. PMID: 17971012

65. Trousdale RK, Jacobs S, Simhaee DA, Wu JK, Lustbader JW. Wound closure and metabolic parameter variability in a db/db mouse model for diabetic ulcers. J Surg Res. 2009; 151(1):100–7. doi: 10.1016/j.jss.2008.01.023 PMID: 18619614

66. Galiano RD, Michaels Jt, Dobryansky M, Levine JP, Gurtner GC. Quantitative and reproducible murine model of excisional wound healing. Wound Repair Regen. 2004; 12(4):485–92. PMID: 15260814

67. Wong VW, Sorkin M, Glotzbach JP, Longaker MT, Gurtner GC. Surgical approaches to create murine models of human wound healing. J Biomed Biotechnol. 2011; 2011:969618. doi: 10.1155/2011/969618 PMID: 21151647

68. Bensebaa F, Andre JJ. Effect of oxygen on phthalocyanine radicals. 1. ESR study of lithium phthalocyanine spin species at different oxygen concentrations. J Phys Chem. 1992; 96(14):5739–45.

69. Bensebaa F, Petit P, André JJ. The effect of oxygen on phthalocyanine radicals II. Comparative study of two lithium phthalocyanine powder derivatives by continuous and pulsed ESR. Synth Met. 1992; 52 (1):57–69.

70. Greenhalgh DG. Tissue repair in models of diabetes mellitus. A review. Methods Mol Med. 2003; 78:181–9. PMID: 12825271

71. Rebalka IA, Raleigh MJ, D'Souza DM, Coleman SK, Rebalka AN, Hawke TJ. Inhibition of PAI-1 via PAI-039 improves dermal wound closure in diabetes mellitus. Diabetes. 2015.

72. Ruzehaji N, Kopecki Z, Melville E, Appleby SL, Bonder CS, Arkell RM, et al. Attenuation of flightless I improves wound healing and enhances angiogenesis in a murine model of type 1 diabetes. Diabetologia. 2014; 57(2):402–12. doi: 10.1007/s00125-013-3107-6 PMID: 24292564